Enhanced α-γ Discrimination in Co-doped $LaBr_3$:Ce

Kan Yang, *Member, IEEE,* Peter R. Menge, *Member, IEEE,* and Vladimir Ouspenski

***Abstract*– $LaBr_3$:Ce crystal scintillator can be co-doped with various alkaline earth metals to improve light output and energy resolution of the basic scintillator. Another benefit is improvement of alpha/gamma discrimination via pulse shape analysis. $LaBr_3$:Ce contains a low level of actinium contamination, which produces an alpha particle background. This background is difficult to discriminate from gamma rays. Conversely, the addition of co-dopant into the crystal makes the alpha response much easier to distinguish. $LaBr_3$:Ce,Sr, for example, produces a second, longer decay component in the scintillation pulse when excited by radiation. The amplitude of this second decay component changes in response to a gamma ray versus a heavy charged particle. The change in pulse shape is used to eliminate the alpha background and enable detection of neutron reaction products.**

I. Introduction

A scintillation radiation detector is more useful when it can distinguish between different types of incoming radiation such as gamma rays and alpha particles. $LaBr_3$:Ce crystal is one of the best scintillators available for the detection of gamma rays. It has high light yield and excellent energy resolution [1]. However, it has poor ability to distinguish between gamma rays and heavy charged particles, such as alphas [2].

Much current study is underway on co-doped $LaBr_3$:Ce to improve properties such as light output and energy resolution. Co-doping with small concentrations of strontium and other aliovalent elements has shown to improve light output by 30% and reduce the energy resolution to as low as 2.0% (FWHM at 662 keV) [3,4]. Another use for co-doping in $LaBr_3$:Ce has been discovered. Co-doping enhances discrimination between gamma rays and heavy charged particles via pulse shape analysis.

$LaBr_3$:Ce contains a low level of actinium contamination [5], which produces an intrinsic alpha particle background at the rate of 0.2 – 0.8 Bq/cm^3. This background is difficult to separate out of a gamma ray energy spectrum using standard $LaBr_3$:Ce. However, the addition of a small amount of co-dopant into the crystal makes the alpha response much easier to distinguish using pulse shape discrimination. $LaBr_3$:Ce,Sr, for example, produces a second, longer decay component in the scintillation pulse when excited by radiation. This second decay component contains less of the total light pulse when the radiation is a heavy charged particle versus a gamma ray (or electron). The intrinsic alpha particle background can be removed from gamma ray spectra by comparing the magnitude of the second components.

Furthermore, thermal neutron detection and discrimination with $LaBr_3$: Ce + co-dopant is now possible. If the crystal is placed in proximity to a neutron reactive material such as ^{6}LiF or $^{10}B_4C$, a dual neutron/gamma ray detector can be constructed. These neutron reactive materials produce heavy charged particles following neutron absorption. Transport of these particles into $LaBr_3$ creates a signal that is distinguishable from gamma rays.

II. Experimental Setup

Three Ø1" × 1" $LaBr_3$ crystals studied in this research were grown by Saint-Gobain Crystals. The crystals listed in Table 1 were wrapped with Teflon reflector and hermetically packaged in titanium housings with sapphire optical windows on one end. Each crystal was optically coupled to the sapphire window by a clear silicone rubber.

TABLE I. $LaBr_3$ Crystals Tested

Constituent	Dopant(s)*
$LaBr_3$	5% Ce^3
$LaBr_3$	5% Ce^{3+} + 0.50% Ca^{2+}
$LaBr_3$	5% Ce^{3+} + 0.50% Sr^{2+}

*at % in the melt, with respect to La^{3+}

For pulse height spectra measurements, the samples were coupled to an Electron Tubes 9305 photomultiplier tube (PMT) with a modified voltage divider [6] with linear response at high energies. The background spectra were acquired for each sample over a 24 hour span.

For pulse shape analysis, the packaged detectors were coupled to a Photonis XP2020Q PMT by optical grease. PMT anode signals were recorded by a CAEN DT5751 1GHz desktop digitizer for post analysis.

For neutron measurements, the ^{6}LiF surrounded detector was coupled to the same Photonis XP2020Q PMT by optical grease. ^{252}Cf was used as the neutron source. High density polyethylene (HDPE) and Pb shielding were inserted between the source and the detector to serve as neutron moderator and gamma ray attenuator, respectively.

III. Results and Discussions

A. Radiation Background in Co-doped $LaBr_3$

The internal radiation background in $LaBr_3$ comes from two major sources. First is the naturally occurring radiative isotope

Manuscript received December 19, 2014.

Kan Yang is with Saint-Gobain Crystals, Hiram OH 44234 USA (telephone: 440-834-5697, e-mail: kan.yang@saint-gobain.com).

Peter R. Menge is with Saint-Gobain Crystals, Hiram OH 44234 USA

Vladimir Ouspenski is with Saint-Gobain Recherche, 39 Quai Lucien Lefranc 93303 Aubervilliers France.

978-1-4799-6097-2/14/$31.00 ©2014 IEEE

^{138}La with 0.090% natural abundance. ^{138}La decays through either electron capture or β^- decay and emits two γ rays at 1435.8 keV and 788.7 keV. A coinciding electron is also emitted with the 788.7 keV gamma ray forming the beta continuum [7]. The 1435.8 keV gamma ray often coincides with the ^{138}Ba K_α x-ray forming a sum peak near 1468 keV [8,9]. A lower energy peak near 1440 keV is formed by the 1435.8 keV gamma coinciding with the L and M cascade x-rays [9]. The second source for internal radiation comes from ^{227}Ac contamination. ^{227}Ac and many of its daughter particles undergo α decay and emit α particles with a variety of energies [5].

As is shown in the energy spectrum in Fig. 1a, the counts in the region below 1.5 MeV are mostly from the internal γ and β from ^{138}La. The counts between approximately 1.7 and 2.7 MeV are from the α particles from ^{227}Ac decay chain.

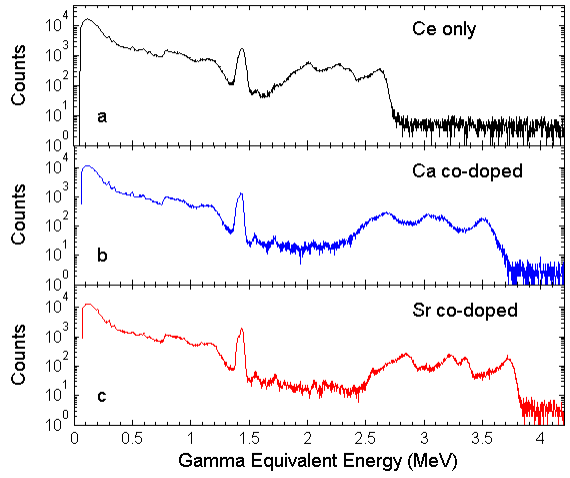

Fig. 1. Pulse height spectra of radiation background for Ce only and co-doped $LaBr_3$:Ce samples. The gamma equivalent energy of alpha particles is increased with co-doping.

The concentration of co-dopants (Ca and Sr) in the matrix is low (0.5 at% in the melt) and neither co-dopant has naturally occurring radioisotopes. Thus, the physical nature of radiation background of co-doped crystals should be the same as that of Ce only $LaBr_3$. However, the background pulse height spectra of co-doped $LaBr_3$:Ce are found to be significantly different from that of Ce only $LaBr_3$. As is shown in Figs. 1b and 1c, the gamma equivalent energies (G.E.E.) of the ^{227}Ac alpha peaks are increased significantly by Ca or Sr co-doping. While the alpha counts appear at 1.7-2.7 MeV in LaBr3:Ce, they appear at 2.3-3.6 MeV for Ca co-doping and 2.5-3.8 MeV for Sr co-doping.

This increase can be precisely gauged by the highest alpha peak, which is from the decay of ^{215}Po in the ^{227}Ac decay chain, which emits an alpha with an energy of 7.386 MeV [5]. The G.E.E. of the ^{215}Po α peak is shifted from 2.63 MeV in Ce only $LaBr_3$ to 3.51 MeV in Ca co-doped $LaBr_3$:Ce and to 3.72 MeV in Sr co-doped $LaBr_3$:Ce. In other words, the scintillation light yield of $LaBr_3$:Ce, when excited by α particles, is increased by 33.5% by Ca co-doping and 41.4% by Sr co-doping relative to the gamma ray light yield.

Heavy charged particles are known to produce high *dE/dx*. Increased scintillation light yield for heavy charged particles indicates reduced non-linear quenching at high excitation density, which is associated with improved non-proportionality [10, 11]. It has been shown that the gamma non-proportionality of $LaBr_3$:Ce, especially its low energy response (i.e. high *dE/dx*), is improved by Ca and Sr co-doping [12]. Improved alpha G.E.E. agrees well with this conclusion.

B. Pulse Shape Analysis

A pulse shape discrimination (PSD) technique was used to determine if the changes in G.E.E. for α events are also associated with changes in their pulse shapes. A Fourier Transform based PSD algorithm was used to extract the pulse shape information for each individual scintillation pulse. The PSD ratio (a.k.a. pulse shape descriptor) is defined by the ratio between the amplitude of the principal frequency component and the amplitude sum of all frequency components of the transformed Fourier spectrum. A large PSD ratio roughly corresponds to a slow pulse. This method is inherently insensitive to noise and the "walk" of pulse trigger due to pulse height variation, which is one of the major uncertainty contributors for PSD algorithms based on the selection of precise time windows (e.g. charge comparison).

Figs. 2-4 present the PSD results for all three crystals. Fig. 2a shows the PSD scatter plot for Ce only $LaBr_3$. Note that the α region (the three "islands" between 1.7 to 2.7 MeV) is slightly shifted above the γ (and β) region in terms of PSD ratio. This indicates that even in Ce only $LaBr_3$, there is a pulse shape difference between α and γ pulses. A similar feature was previously observed but was too small to be useful [2]. A PSD Figure of Merit (FOM) [13] can be used to quantify the quality of discrimination between α and γ. In the case of $LaBr_3$:Ce, the FOM is calculated to be 0.73 with energy threshold set at 1.6 MeV. This PSD FOM is too low to for any practical application.

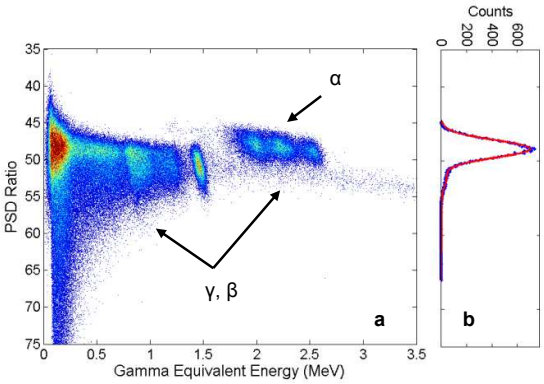

Fig. 2. a) PSD scatter plot of $LaBr_3$:Ce radiation background; b) PSD spectrum of α and γ events

However, both Ca and Sr co-doped $LaBr_3$ crystals show significantly improved PSD performance. As is shown in Figs. 3 and 4, in addition to the increased G.E.E., the α events in both co-doped $LaBr_3$ crystals are more clearly separated from

the γ events. With the same energy threshold, the PSD FOM is determined to be 1.25 for $LaBr_3$:Ce,Ca and 1.57 for $LaBr_3$:Ce,Sr. With FOM > 1.5, complete separation can be achieved. [14].

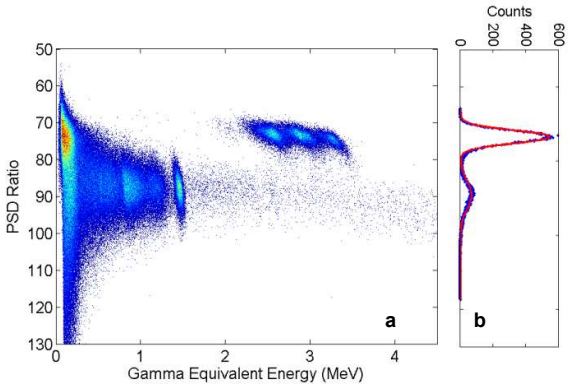

Fig. 3. a) PSD scatter plot of $LaBr_3$:Ce, Ca radiation background; b) PSD spectrum of α and γ events

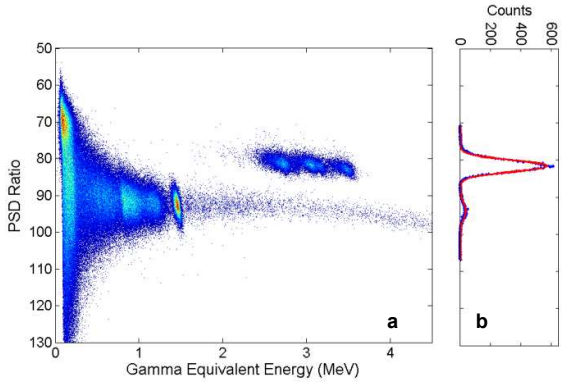

Fig. 4. a) PSD scatter plot of $LaBr_3$:Ce, Sr radiation background; b) PSD spectrum of α and γ events

By normalizing and averaging all the α and γ pulses within corresponding energy ranges on the PSD scatter plot, the detailed pulse shape differences can be resolved. Fig. 5 illustrates the pulse shape difference between the α pulse and the γ pulse in all three crystals. Even for the Ce only $LaBr_3$ (Fig. 5a), the γ pulse appears to have a very small amount of secondary component, which makes it last slightly longer than the α pulse. The secondary long component has much stronger presence in both Ca and Sr co-doped $LaBr_3$:Ce than the Ce only $LaBr_3$ [12, 15].

As is shown in Figs. 5b and 5c, the difference between α and γ pulses of co-doped crystals is much more prominent than that of Ce only crystals. The α pulse shows significantly less secondary component than the γ pulse. This difference serves as the basis for enhanced PSD. Table II compares the percentage of light in secondary decay component for all three crystals.

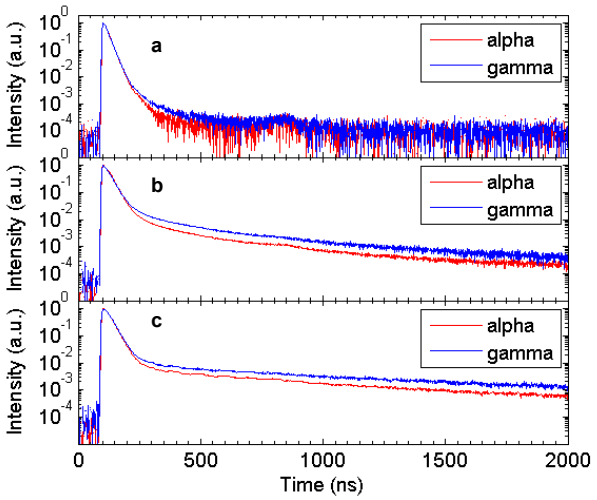

Fig. 5. Averaged PMT pulses of a) $LaBr_3$:Ce, b) $LaBr_3$:Ce.Ca and 3) $LaBr_3$:Ce.Sr

TABLE II. PERCENTAGE OF LIGHT IN SECONDARY DECAY COMPONENT

Particule Type	Ce only	Ce + Ca co-doped	Ce + Sr co-doped
α	1.2%	6.3%	9.5%
γ	2.1%	12.7%	15.1%

C. *Background Suppression*

With enhanced pulse shape differences, it is now possible to completely eliminate the α background from co-doped $LaBr_3$:Ce. Fig. 6 illustrates the background spectrum of Sr co-doped $LaBr_3$:Ce with α rejection. Compare this to Fig. 1c. Based on the fact that the α-γ FOM is 1.57, the rejection ratio is estimated to be 10^{-8}. It is worth noting that with α rejection, the crystal is even able to resolve the weak 2.615 MeV γ ray from ^{232}Th in the surrounding environment.

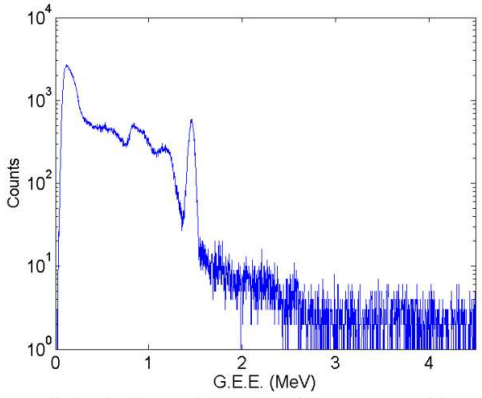

Fig. 6. Radiation background spectrum of $LaBr_3$:Ce, Sr with α rejection

D. *Neutron-Gamma Dual Detection*

Since co-doped $LaBr_3$:Ce is able to discriminate heavy charged particles from γ photons, it is possible to construct a thermal neutron – gamma dual detector by utilizing this new feature. If co-doped $LaBr_3$:Ce is placed in the vicinity of a neutron converter material like ^{10}B or ^{6}Li, it should be able to

detect and discriminate the heavy charged particles emitted by ^{6}Li neutron capture. The neutron capture reaction on ^{6}Li emits a triton with 2.75 MeV and an α particle with 2.05 MeV energy:

$n + {}^{6}Li \rightarrow t\ (2.75\ MeV) + \alpha\ (2.05\ MeV)$

Similar to the internal α particles from ^{227}Ac decay chain, Sr co-doped $LaBr_3$:Ce should be able to differentiate both triton and α particle from γ photons.

A prototype detector was constructed by surrounding a ⌀ 1" × 1" Sr co-doped $LaBr_3$:Ce crystal with 93.5% enriched ^{6}LiF powder. A schematic drawing is shown in Fig. 7. ^{6}LiF powder was used as both a neutron sensing layer and a light reflector. The energy resolution of this particular prototype detector is 2.79% at 662 keV. No degradation of γ response is observed, due to the excellent reflectivity of LiF powder

The thickness of the ^{6}LiF powder layers is approximately 2 mm, which is much thicker than the short range of tritons and α particles in LiF. Based on MCNP simulations, the range for a 2.75 MeV triton in LiF is ~ 28 μm and the range for a 2.05 MeV α particle in LiF is ~ 7 μm [16]. Tritons and alphas originating near the outer surface of ^{6}LiF layer may lose part or all of their energies before reaching the $LaBr_3$ crystal.

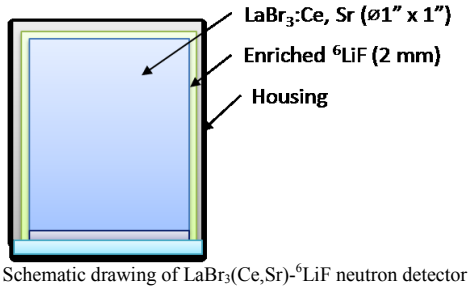

Fig. 7. Schematic drawing of $LaBr_3$(Ce,Sr)-^{6}LiF neutron detector

The PSD scatter plot for the neutron measurement is shown in Fig. 8. The same Fourier Transform based PSD algorithm was used for this pulse shape analysis. Similar to the previous PSD scatter plots, the γ pulses form a "band" which spans the entire recorded energy range. The "γ band" is not completely parallel to the x-axis but "bends" downward slightly at high energies. This is believed to be a result of current saturation in the PMT. The gamma peak near 2.2 MeV is from the hydrogen-neutron capture reaction in the surrounding moderator. Two neutron related features are observed in the scatter plot, one is the parallelogram-shaped region between 1 and 2 MeV G.E.E. The other one is the region between 60 and 80 PSD ratio and between 0.5 and 1 MeV G.E.E. The first group of events is from the tritons emitted from the reaction. The second group of events is from the α particles. As is shown in Fig. 8, the neutron signals (triton) can be clearly separated from the γ signal with a valley in between. However, signals of α particles from ^{6}Li(n,t)α are more difficult to be discriminated from γ signals mainly due to their lower G.E.E.

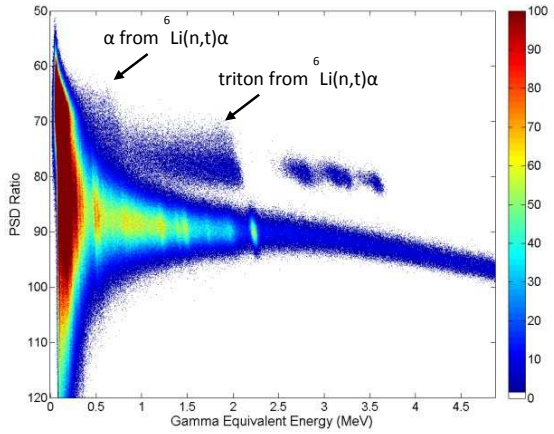

Fig. 8. PSD scatter plot for $LaBr_3$(Ce,Sr) – LiF detector excited by ^{252}Cf

It is possible to create a pulse height spectrum of all heavy charged particles by separating them at the upper contour curve of the γ band. It should be noted that the counts of α events at low energies are underestimated because a large portion of them are indistinguishable from γ events. Fig. 9 shows such a spectrum. The endpoint G.E.E. for α particles is around 0.9 MeV which corresponds to the full energy α particle at 2.05 MeV from ^{6}Li(n,t)α. It does not appear to be feasible to use the α signal alone as a neutron indicator due to its significant overlap with γ signals. The triton peak shows an endpoint G.E.E. around 2.1 MeV which corresponds to the full energy triton at 2.75 MeV. Light output under triton excitation is much less quenched than that under α particle excitation in $LaBr_3$, due to its lower *dE/dx*. It is feasible to use the triton signal alone for neutron detection. As expected, energy straggling is observed. The full energy triton peak has a large "shoulder" area on the low energy side. Reducing the thickness of ^{6}LiF layer is expected to reduce straggling and create a more defined peak.

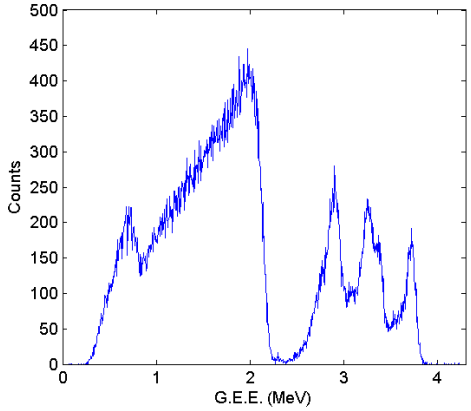

Fig. 9. Pulse height spectrum for heavy charged particles from ^{6}Li(n,t)α reaction.

In order to estimate the FOM for n-γ PSD, the upper and lower energy threshold is set at 2.2 and 1.8 MeV, respectively. The PSD spectrum is shown in Fig. 10. A clear separation is

seen between the neutron and gamma PSD peaks. The FOM is calculated to be 1.22.

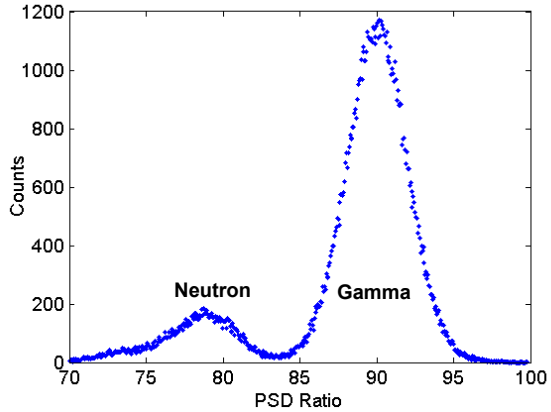

Fig. 10. Neutron-gamma PSD spectrum for $LaBr_3$(Ce,Sr)-^{6}LiF detector

IV. Summary

Both Ca and Sr co-doping increase the Gamma Equivalent Energy for heavy charged particles in $LaBr_3$:Ce. Pulse shape discrimination between α particles and γ ray photons is also significantly enhanced by co-doping. Based on this new feature, α background from ^{227}Ac can now be completely eliminated by a PSD technique.

Using a ^{6}LiF conversion layer, Sr co-doped $LaBr_3$:Ce can be a high-performance dual mode detector for both neutrons and gammas. Thickness of the ^{6}LiF layer and the geometry of $LaBr_3$:Ce will be further optimized in future work to improve detection efficiency and reduce energy straggling.

References

[1] E.V.D. van Loef, P. Dorenbos, C.W.E. van Eijk, K. Kramer, and H.U.Godel, Appl. Phys. Lett., 79, pp. 1573-1575 (2001).

[2] C. Hoel, L.G. Sobotka, K.S. Shah, J. Glodo, Nucl. Instrum. Meth. A, 540 pp. 205-208 (2005).

[3] K. Yang, P.R. Menge, J. Buzniak, V. Ouspensiki, 2012 IEEE-NSS-MIC Conference record, N1-135, pp. 308-311 (2012).

[4] M. S. Alekhin, J. T. M. de Haas, I. V. Khodyuk, K. W. Krämer, P. R. Menge, V. Ouspenski and P. Dorenbos, Appl. Phys. Lett. 102, 161915 (2013).

[5] B.D. Milbrath, R.C. Runkle, T.W. Hossbach, W.R. Kaye, E.A. Lepel, B.S. McDonald, L.E. Smith, Nucl. Instrum. Meth. A, 547, pp. 504–510 (2005).

[6] P. R. Menge, G. Gautier, A. Iltis, C. Rozsa, and V. Solovyev, Nucl. Instrum. Meth. A, vol. 579, pp. 6-10, (2007).

[7] L.P. Ekström and R.B. Firestone, WWW Table of Radioactive Isotopes, database version 2/28/99 , http://ie.lbl.gov/toi/index.htm

[8] B.D. Milbrath, J.I. McIntyre, R.C. Runkle, and L.E. Smith IEEE Trans. Nucl. Sci., vol. 53, no. 5, pp. 3031-3034 (2006).

[9] F.G.A. Quarati, I.V. Khodyuk, C.W.E. van Eijk, P. Quarati, P. Dorenbos, Nucl. Instrum. Meth. A, 683, pp. 46–52 (2012).

[10] R. B. Murray and A. Meyer, Phys. Rev., vol. 122, no. 3, p. 815 (1961).

[11] R. T. Williams, Joel Q. Grim, Qi Li, K. B. Ucer, and W. W. Moses, Phys. Status Solidi B 248, No. 2, 426–438 (2011).

[12] M. S. Alekhin, J. T. M. de Haas, I. V. Khodyuk, K. W. Krämer, P.R. Menge, V. Ouspenski, and P. Dorenbos, Applied Physics Letters, 102, 161915 (2013).

[13] K. Yang, P.R. Menge, Nucl. Instrum. Meth. A, Available online 6 September 2014, ISSN 0168-9002, http://dx.doi.org/10.1016/j.nima.2014.08.031.

[14] R.A. Winyard, J.E. Lutkin, G.W. McBeth, Nucl. Instrum. Meth., vol. 95, issue 1, Pages 141-153 (1971).

[15] M. S. Alekhin, D. A. Biner, K. W. Krämer, and Dorenbos, P., Journal of Applied Physics, 113, 224904 (2013).

[16] D. B. Pelowitz, Ed., "MCNPX User's Manual," Los Alamos National Laboratory, NM Version 2.7.0. Tech. Rep. LA-CP-11-00438, (2011).